Monthly Notices
of the
ROYAL ASTRONOMICAL SOCIETY

MNRAS **494,** 3663–3674 (2020)
Advance Access publication 2020 April 8

doi:10.1093/mnras/staa958

The observed velocity distribution of young pulsars – II. Analysis of complete PSRπ

Andrei P. Igoshev ★

Department of Applied Mathematics, University of Leeds, Leeds LS2 9JT, UK

Accepted 2020 April 2. Received 2020 April 2; in original form 2019 November 14

ABSTRACT

Understanding the natal kicks, or birth velocities, of neutron stars is essential for understanding the evolution of massive binaries and double neutron star formation. We use maximum likelihood methods as published in Verbunt et al. to analyse a new large data set of parallaxes and proper motions measured by Deller et al. This sample is roughly three times larger than number of measurements available before. For both the complete sample and its younger part (spin-down ages $\tau < 3$ Myr), we find that a bimodal Maxwellian distribution describes the measured parallaxes and proper motions better than a single Maxwellian with probability of 99.3 and 95.0 per cent, respectively. The bimodal Maxwellian distribution has three parameters: fraction of low-velocity pulsars and distribution parameters σ_1 and σ_2 for low- and high-velocity modes. For a complete sample, these parameters are as follows: 42^{+17}_{-15} per cent, $\sigma_1 = 128^{+22}_{-18}$ km s^{-1}, and $\sigma_2 = 298 \pm 28$ km s^{-1}. For younger pulsars, which are assumed to represent the natal kick, these parameters are as follows: 20^{+11}_{-10} per cent, $\sigma_1 = 56^{+25}_{-15}$ km s^{-1}, and $\sigma_2 = 336 \pm 45$ km s^{-1}. In the young population, 5 ± 3 per cent of pulsars have velocities less than 60 km s^{-1}. We perform multiple Monte Carlo tests for the method taking into account realistic observational selection. We find that the method reliably estimates all parameters of the natal kick distribution. Results of the velocity analysis are weakly sensitive to the exact values of scale lengths of the Galactic pulsar distribution.

Key words: methods: data analysis – methods: statistical – stars: neutron – pulsars: general.

1 INTRODUCTION

The origin of pulsar velocities is of profound importance to many areas of astrophysics. Of particular interest is the distribution of *natal kicks*. Natal kicks are defined here as the velocity received by neutron star (NS) in excess to its progenitor local standard of rest (LSR) velocity (if formed from isolated massive star), or as the velocity received by the NS, which disrupted a binary in excess to the LSR velocity of the binary centre of mass. It was shown by Kuranov, Popov & Postnov (2009) that even in the case of binary origin the observed space velocities are mostly affected by the natal kick velocity distribution and not by binary evolution. NSs are known to receive natal kicks at the moment of supernova explosion (Podsiadlowski, Pfahl & Rappaport 2005). This fact is derived from observations of large peculiar velocities (order of 100 km s^{-1}) of isolated radio pulsars in comparison to their progenitors OB stars with peculiar velocities of ≈10–15 km s^{-1} (Lyne & Lorimer 1994). The young NSs are known to be located at some offset from the centre of the associated supernova remnants (SNRs; Frail, Goss & Whiteoak 1994; Holland-Ashford et al. 2017). Some NSs demonstrate a bow shock as a proof of direct association of the pulsar with the SNR and large pulsar speed, e.g. the Guitar Nebula (Cordes, Romani & Lundgren 1993). The scale height of radio pulsar population in the Galaxy (330 pc; Lorimer et al. 2006) is much larger than the scale height of pulsar progenitors (≈50 pc). These multiple direct observations confirm a large natal kick scenario for a significant number of NSs.

There are certain indications that some NSs received very small natal kicks. In particular, the formation of some double NSs systems requires natal kicks of order of tens km s^{-1} (Tauris et al. 2017). Mapelli & Giacobbo (2018) used binary population synthesis coupled together with cosmological simulation to study dependence of double NSs merger rate on natal kicks. They found that it was necessary to assume extremely small value of $\sigma = 15$ km s^{-1} for the Maxwellian velocity distribution to reproduce the double NSs merger rate derived from the gravitational wave detection GW170817 (Abbott et al. 2017). There is a group of Be X-ray binaries with small eccentricities and large orbital periods (Pfahl et al. 2002; Townsend et al. 2011) that requires natal kicks of $v <$ 50 km s^{-1} to explain their observational properties. This indirect evidence suggests that a noticeable fraction of NSs are born with small natal kicks.

Knowledge of the natal kick distribution for NSs is important because it is an essential ingredient of models for double NSs formation, in particular the double NS mergers (Abbott et al. 2017),

★ E-mail: ignotur@gmail.com

Table 1. Sources for parallaxes and proper motions in our master list. N is a number of objects with $\varpi'/\sigma_{\varpi} > 3$ and n is a number of those younger than 3 Myr.

S	Source		N	n
1	Brisken et al. (2002)	table 4	4	0
2	Brisken et al. (2003)	table 3	1	1
3	Chatterje et al. (2001)	table 2	1	1
4	Chatterjee et al. (2004)	table 1	1	1
5	Deller et al. (2009)	table 3	3	1
6	Chatterjee et al. (2009)	table 2	11	5
7	Kirsten et al. (2015)	table 5	3	2
8	Deller et al. (2019)	table 3	45	10
		Total	69	21

short gamma-ray bursts, millisecond pulsars formation, and different scenarios for white dwarfs (WDs)–NS mergers (Toonen et al. 2018). Natal kicks are essential to model the Galactic distribution of pulsars and eventually design radio surveys to discover new NSs. A fraction of low-velocity NSs are important to predict and interpret (if discovered) a fraction of NSs accreting from the interstellar medium (Ostriker, Rees & Silk 1970; Shvartsman 1971). For example, Popov et al. (2000) derived the lower bound on the mean kick velocity as 200–300 km s^{-1} based on absence of isolated accreted NSs sources in the *ROSAT* observations. Future observations with the *eROSITA* mission (Predehl et al. 2011), which is much more sensitive than *ROSAT* and should discover multiple isolated accreted NSs, will help solving this issue (Popov, Postnov & Shakura 2015).

One of the well-known ideas to constrain the natal kick velocity distribution is to analyse the parallaxes and proper motions of young isolated radio pulsars (see e.g. Arzoumanian, Chernoff & Cordes 2002; Verbunt, Igoshev & Cator 2017). Verbunt et al. (2017) analysed a small sample containing 28 pulsars (19 pulsars with spin-down age less than 10 Myr). They used a maximum likelihood method to estimate parameters of the velocity distribution consistently. This estimate crucially depends on our knowledge of precise parallaxes and proper motions for a large number of objects.

The primary reason for this new study is a recent publication of a large sample of precise interferometric measurements by Deller et al. (2019). This sample contains measurements for 57 radio pulsars; most parallaxes are measured for the first time. We use the same maximum likelihood technique described by Verbunt et al. (2017) to analyse this extended sample combined with older measurements. Therefore, we aim at obtaining a more reliable estimate for the natal kick velocity distribution. We also aim at testing the sensitivity of the method to a particular choice of parameters for Galactic distribution of pulsars and observational selection.

This paper is structured as follows: in Section 2, we describe our data set; in Section 3, we briefly introduce the essential ingredients of the maximum likelihood technique; and in Section 4, we present the results. We conclude our paper with discussion and conclusions.

2 DATA

In this research, we combine new measurements presented by Deller et al. (2019) with older reliable very long baseline interferometry (VLBI) measurements of parallaxes and proper motions previously collected by Verbunt et al. (2017). Table 1 shows the list of literature sources; all the measurements are compiled in the master list (Table A1). To find periods and period derivative of pulsars we use the Australia Telescope National Facility (ATNF) Catalogue (Manchester et al. 2005).[1] In this research, we decide to keep only reliable measurements for parallax, i.e. $\varpi'/\sigma_{\varpi} > 3$, where ϖ' is the measured parallax and σ_{ϖ} is the parallax uncertainty. A cut-off $\varpi'/\sigma_{\varpi} > 2$ or $\varpi'/\sigma_{\varpi} > 4$ removes just one additional pulsar from the list. In principle, our method could deal with upper limits as well, but in this case the final result becomes much more sensitive to exact assumptions about the spatial distribution of the pulsars in the Galaxy. This distribution is based on previous distance measurements (often via the electron density model) and is not particularly reliable for radio pulsars. If the parallax or proper motion uncertainty is non-symmetric, we choose the greatest value out of two.

To update the list we replace parallax and proper motion measurements by Brisken et al. (2002) with values provided by Deller et al. (2019) for two radio pulsars: J0332+5434 (new parallax differs 3.05σ) and J1136+1551 (new parallax differs 0.71σ). Deller et al. (2019) provided parallax measurements for five pulsars from Brisken et al. (2003) with measured proper motions. Three of these pulsars (J1645–0317, J1735–0724, and J2305+3100) are younger than spin-down age $\tau = 10$ Myr. As a measure of the pulsar age we use the spin-down age $\tau = P/(2\dot{P})$, where P is the pulsar period and $\dot{P}$ is the period derivative. The spin-down age could differ from real age if the initial period of pulsar is large or the pulsar experienced a magnetic field evolution. It seems that the spin-down age works reasonably well for most pulsars with $\tau < 10$–20 Myr (Igoshev 2019).

In general our master list includes nearly all objects from Deller et al. (2019) with exception of four millisecond (recycled) radio pulsars (J2010–1323, J2145–0750, J2317+1439, and J1022+1001). We also exclude NSWD system J0823+0159. Binaries with radio pulsars move in respect to the LSR with a peculiar velocity that could significantly differ from the pulsar natal kick because the energy and momentum of the kick are partly redistributed into the orbital parameters. As in the previous research we do not include any pulsars located inside globular clusters. The total number of previous measurements of good quality is 24, while the number of new good quality measurements is 45. We do not extend our sample further to include pulsars with distances based on dispersion measure and an electron density model of the Galaxy as it was shown by Deller et al. (2019) these distances could differ 3–5 times from parallax measurements both for NE2001 (Cordes & Lazio 2002) and YMW16 (Yao, Manchester & Wang 2017) models.

We plot the positions and proper motions for radio pulsars in our master list in Fig. 1. It is easy to notice a dearth of objects around $l = 270$ (possibly because it is unavailable for the VLBI observations). In general we notice objects above and below the Galactic plane. Despite the corrections for motion of LSR being small as it is seen from Fig. 1 (red lines), we take them into account by adopting a flat Galaxy rotation curve with speed $v_{\rm R} = 220$ km s^{-1} and distance of the Sun from the Galactic Centre $\rm R_{\odot} = 8.5$ kpc. Pulsars in the catalogue by Deller et al. (2019) have smaller parallaxes in comparison to previous measurements, see left-hand panel of Fig. 2.

In the right-hand panel of Fig. 2, we plot the cumulative distribution of transverse velocities computed as

$$v_{\perp}\,[\mathrm{km\,s^{-1}}] = \frac{4.74}{\varpi'\,[\mathrm{mas}]}\sqrt{\mu'^2_{\alpha*} + \mu'^2_{\delta}}\,[\mathrm{mas\,yr^{-1}}], \quad (1)$$

where $\mu'_{\alpha*}$ and μ'_{δ} are the measured values of proper motion in the direction of right ascension and declination. We see that the

[1] http://www.atnf.csiro.au/research/pulsar/psrcat

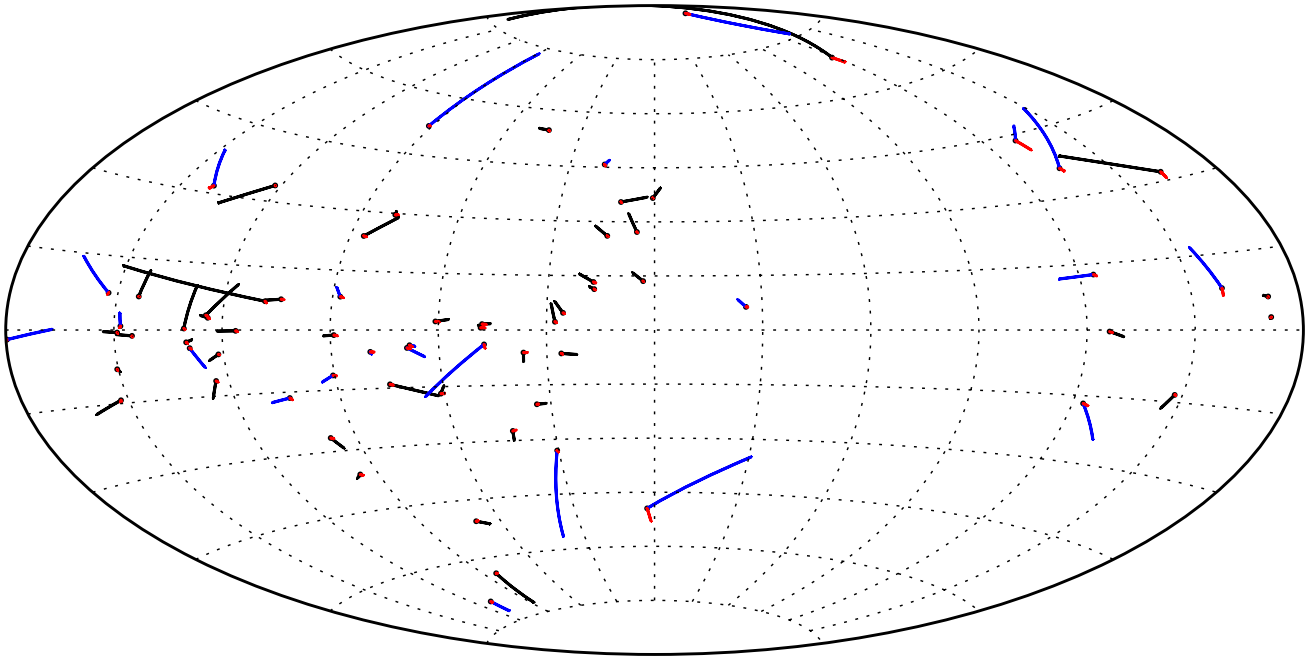

Figure 1. Proper motions of pulsars in 0.5 Myr (blue lines for older measurements, black lines for objects form Deller et al. 2019) in the Galactic coordinate system. Red lines show the proper motion with respect to the local standard of rest (LSR) at each position (see text).

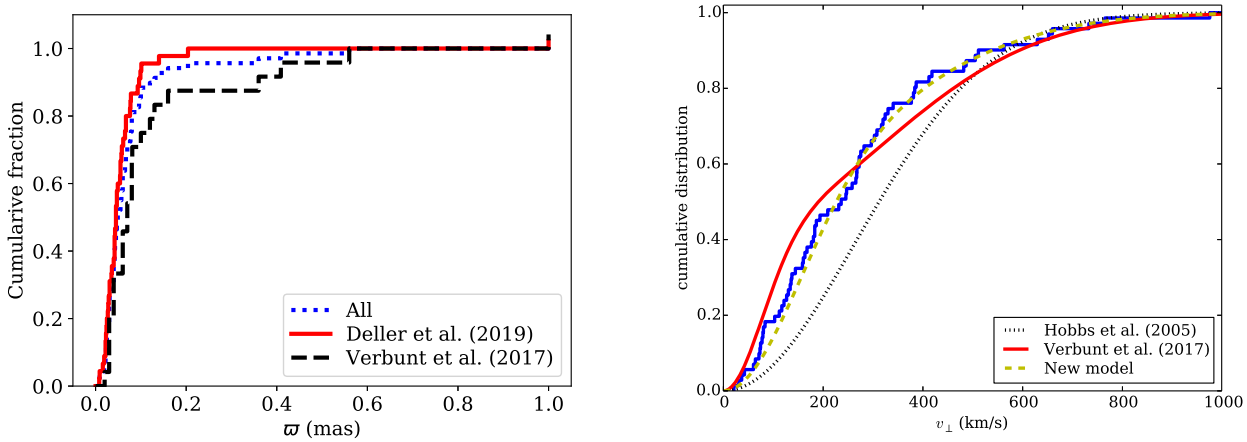

Figure 2. Left-hand panel: cumulative distribution of measured parallaxes for pulsars from Verbunt et al. (2017) (dashed black line), from Deller et al. (2019) (solid red line), and combination of these two catalogues (dotted blue line). Right-hand panel: the cumulative distribution of transverse velocities for radio pulsars with well-measured parallaxes ($\varpi/\sigma_\varpi > 3$; blue histogram) and cumulative velocity distributions presented earlier in Hobbs et al. (2005) (dotted black line) and Verbunt et al. (2017) (solid red line). Dashed yellow line shows result of optimization for all pulsars using the mixed model.

distribution suggested by Hobbs et al. (2005) has a systematic shift, and therefore does not describe the new data. The origin of this systematic shift could be due to overestimated distances to pulsars. The distribution suggested in Verbunt et al. (2017) seems to reliably estimate the low-velocity tail, but somewhat differs from the data in the regions around ≈100 and ≈400 km s^{-1}.

3 METHOD

We use the same maximum likelihood methods as described in Verbunt & Cator (2017) and Verbunt et al. (2017), therefore, we refer any interested reader to these two articles for detailed description. Here we give a brief summary highlighting most relevant details.

3.1 The Galactocentric pulsar distribution

We assume that the Galactic distribution of pulsars forms a thin, exponential disc. In this assumption we follow the previous works of Verbiest et al. (2012) and Lorimer et al. (2006) with corrections of Igoshev, Verbunt & Cator (2016). The exact form of the distribution is

$$f_D(D)\,\mathrm{d}D = C D^2 R^{1.9} \exp\left[-\frac{|z|}{h} - \frac{R}{H}\right] \mathrm{d}D, \quad (2)$$

where $|z|$ is the height of a pulsar above the Galactic plane, C is the normalization factor, and R is the Galactocentric distance of the pulsar. Two values h and H are parameters of the model; for young radio pulsars these values are usually assumed to be $h = 0.33$ kpc and $H = 1.7$ kpc. Given the wealth of interferometric data provided

by Deller et al. (2019), we aim to optimize these parameters. Equation (2) is normalized numerically for each direction and each set of parameters h, H for $D \in [0, 10]$ kpc, such that

$$\int_0^{10} f_D(D)\,\mathrm{d}D = 1. \tag{3}$$

This step is essential if parameters h and H are optimized using the maximum likelihood technique.

3.2 Velocity distributions

We analyse four different velocity distributions $f_v(\boldsymbol{v}|\boldsymbol{\sigma})\,\mathrm{d}v$ with vector of parameters $\boldsymbol{\sigma}$. First, we use isotropic Maxwellian velocity distribution[2] with a single parameter σ,

$$f_{v,\mathrm{maxw}}(\boldsymbol{v}|\sigma)\,\mathrm{d}v = \sqrt{\frac{2}{\pi}}\frac{v^2}{\sigma^3}\exp\left[-\frac{v^2}{2\sigma^2}\right]\mathrm{d}v; \qquad (0 < v < \infty). \tag{4}$$

Second, we use a sum of two isotropic Maxwellian distributions (the so-called bimodal Maxwellian distribution):

$$f_{v,\mathrm{2maxw}}(\boldsymbol{v}|w,\sigma_1,\sigma_2)\,\mathrm{d}v = w f_{v,\mathrm{maxw}}(\boldsymbol{v}|\sigma_1) + (1-w) f_{v,\mathrm{maxw}}(\boldsymbol{v}|\sigma_2)\,\mathrm{d}v, \tag{5}$$

where w is a fractional contribution of the first Maxwellian, such that $w \in [0, 1]$. If $w = 0$ or $w = 1$, the distribution defined by equation (5) becomes a single Maxwellian.

Third, we introduce a mixed model that is a combination of isotropic and a semi-isotropic Maxwellian distribution $f_{v,\mathrm{semi}}(\boldsymbol{v}|\sigma)\,\mathrm{d}v$. The latter one is a Gaussian distribution for velocity component directed away from the Galactic plane ($v_z\, z > 0$) and zero otherwise, two other velocity components are not affected. The motivation for this model is as follows: young pulsars born in the Galactic plane with velocities pointing outside the plane move for some time (30–100 Myr) in the same direction as their original velocity vector. Meaning that if a young pulsar is discovered at positive galactic latitude $b > 0$, most probably its μ_b is also positive. An older pulsar could also move towards the plane because its velocity was altered significantly by the Galactic gravitational potential. Therefore we cannot apply the semi-isotropic model to them. This model is a good first test for probing the natal kick velocity orientation in the younger sample. If the semi-isotropic model provides a better fit than the isotropic model, it means that their speeds were not significantly altered by Galactic gravity. The model is

$$f_{v,\mathrm{semi}}(\boldsymbol{v}|\sigma)\,\mathrm{d}v = \begin{cases} 2\sqrt{\frac{2}{\pi}}\frac{v^2}{\sigma^3}\exp\left[-\frac{v^2}{2\sigma^2}\right]\mathrm{d}v, & \text{if } v_z\, z > 0, \\ 0, & \text{otherwise.} \end{cases} \tag{6}$$

We call it a mixed velocity distribution because we apply the isotropic Maxwellian distribution to one group of pulsars and semi-isotropic Maxwellian distribution to another group. The first group (isotropic) contains 17 pulsars with no clear preference for orientation of the velocity vector. The second group (semi-isotropic) contains 52 pulsars with expected motion directed away from the Galactic plane. The second group consists of young and intermediate age pulsars (spin-down age $\tau < 50$ Myr with nominal height $|z| = |\sin b/\varpi'| > 50$ pc), first group includes all remaining pulsars.

[2]The Maxwellian velocity distribution is isotropic by definition, but because we want to study a modified Maxwellian distribution made anisotropic, we highlight this fact.

Fourth, we combine two mixed Maxwellian distributions:

$$f_{v,\mathrm{2mix}}(\boldsymbol{v}|w,\sigma_1,\sigma_2)\,\mathrm{d}v = w f_{v,\mathrm{mix}}(\boldsymbol{v}|\sigma_1) + (1-w) f_{v,\mathrm{mix}}(\boldsymbol{v}|\sigma_2)\,\mathrm{d}v. \tag{7}$$

This model is analogous to model that consists of two isotropic Maxwellians. It is introduced here to test if the sample is indeed kinematically young.

3.3 The likelihood function and model comparison

Using equation (2) and one of velocity distributions equations (4)–(7) together with normal distributions for measurement errors for parallax $g_\varpi(\varpi'|D)$ and two components of proper motion $g_\mu(\mu'_{\alpha*}|\boldsymbol{v}, D)$, $g_\mu(\mu'_\delta|\boldsymbol{v}, D)$, we compute the joint probability $P(\varpi', \mu'_{\alpha*}\mu'_\delta, \boldsymbol{v}, D|\boldsymbol{\sigma})$. The joint probability depends on unknown actual distance D and velocity vector $\boldsymbol{v}$, so we integrate it over these quantities partly numerically and partly analytically to produce the conditional probability of individual measurements given a parameter of the particular velocity distribution:

$$P(\varpi', \mu'_{\alpha*}\mu'_\delta|\boldsymbol{\sigma}) = \iiiint P(\varpi', \mu'_{\alpha*}\mu'_\delta, \boldsymbol{v}, D|\boldsymbol{\sigma})\,\mathrm{d}^3\boldsymbol{v}\,\mathrm{d}D. \tag{8}$$

We assume that the measurements of individual pulsars do not depend of each other, in this case the conditional probabilities for different pulsars can be multiplied to form a likelihood of the model given the data. Doing so, we also assume that the proper motion measurement is independent of the parallax measurement. Measurements of proper motion might correlate with parallax measurements but the value of this correlation is not currently provided in the data sets. For numerical convenience we compute the logarithm of the likelihood,

$$\mathcal{L}(\boldsymbol{\sigma}) = -2\sum_{i=0}^{N}\log P(\varpi', \mu'_{\alpha*}\mu'_\delta|\boldsymbol{\sigma}). \tag{9}$$

We further optimize the log-likelihood for every velocity distribution and find the best parameters $\hat{\sigma}$.

We use the log-likelihood difference,

$$\Delta\mathcal{L} = \mathcal{L}(\sigma) - \mathcal{L}(\hat{\sigma}), \tag{10}$$

in each direction of the parameter vector $\boldsymbol{\sigma}$ to estimate the confidence interval. The log-likelihood difference of $\Delta\mathcal{L} = 1$ approximately corresponds to a 68 per cent confidence region.

To compare two velocity distributions given the same data set (with respective log-likelihoods $\mathcal{L}^a(\hat{\sigma}_1)$ and $\mathcal{L}^b(\hat{\sigma}_2)$), we compute log-likelihood difference of these models,

$$d\mathcal{L} = \mathcal{L}^a(\hat{\sigma}_1) - \mathcal{L}^b(\hat{\sigma}_2). \tag{11}$$

This is the likelihood ratio test, which follows the asymptotic of χ^2 distribution with number of parameters equal to number of additional free variables present in the second model in comparison to the first model. We illustrate the model comparison in Fig. 3. The likelihood function for a model with a single Maxwellian reaches maximum around 300 km s^{-1} with a value of log-likelihood $2\mathcal{L} = -467$. On the other hand, the likelihood function for sum of two isotropic Maxwellians reaches higher maximum at $\sigma_2 \approx$ 340 km s^{-1} with $2\mathcal{L} = -461$. The likelihood difference $d\mathcal{L} = 6$. Thus the model with a single Maxwellian distribution is rejected at the level of 5 per cent because $\chi^2 = 6$ corresponds to 95 per cent probability for two degrees of freedom. The usage of the likelihood ratio test is justified for comparison of models consistent of two Maxwellians versus a single Maxwellian since these are nested

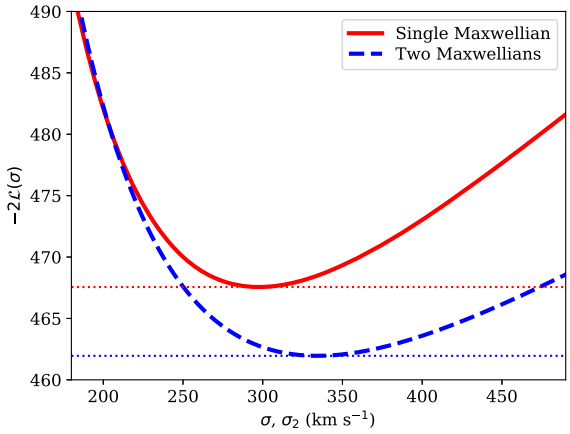

Figure 3. The log-likelihood profile for Y sample for model with a single isotropic Maxwellian distribution (red solid curve) and a sum of two isotropic Maxwellian distributions (blue dashed line). In the case of the latter model we fix $w = 0.19$ and $\sigma_1 = 55$ km s^{-1}. The minima are indicated by horizontal dotted lines for each case.

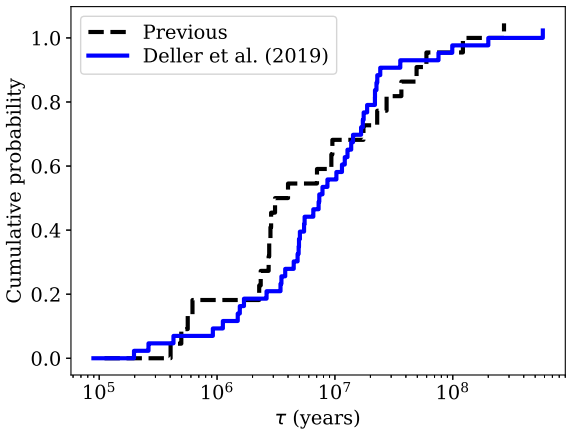

Figure 4. Cumulative distribution of spin-down ages for pulsars in sample of Verbunt et al. (2017) (black dashed line) and in the sample of Deller et al. (2019) (solid blue line).

models, i.e. two Maxwellians can approximate a single Maxwellian distribution if parameters are chosen in a particular way. We confirm that the likelihood ratio test works for model comparison using Monte Carlo tests described in Appendix B.

4 RESULTS

4.1 Velocity distribution of all radio pulsars

We show the results of our analysis in Table 2. Overall, a Maxwellian with $\sigma = 229^{+16}_{-14}$ km s^{-1} fits the distribution. Verbunt et al. (2017) give an estimate of $\sigma = 244$ km s^{-1} that is within the 68 per cent confidence interval. In comparison to that work, the confidence interval shrunk from ≈50 to ≈30 km s^{-1} as the number of pulsars in the sample increased. The result of Hobbs et al. (2005) ($\sigma = 265$ km s^{-1}) is outside of 68 per cent confidence interval, but is within 99 per cent confidence interval.

When we use the isotropic bimodal Maxwellian distribution, we get following result: 58^{+10}_{-11} per cent of objects are drawn from the Maxwellian distribution with $\sigma_1 = 146^{+16}_{-21}$ km s^{-1} and 42^{+11}_{-10} per cent from the Maxwellian with $\sigma_2 = 317^{+29}_{-40}$ km s^{-1}. The contours of constant likelihood are shown in Fig. 5 (upper left-hand panel). The most probable σ_1 correlates with the contribution of the first component w: the lower w, the lower σ_1 should be. It could indicate that the actual distribution is not a sum of two Maxwellians, but instead it could be described by two separate variables. While the contribution and location of the high-velocity component are roughly consistent with the result of Verbunt et al. (2017) (within the 68 per cent confidence interval), the low-velocity component is inconsistent. We notice that the sample compiled by Deller et al. (2019) strongly lacks low-velocity pulsars especially with large spin-down ages. While the sample of Brisken et al. (2002) contained two out of nine pulsars (roughly 22 per cent) with nominal transverse velocity less than 40 km s^{-1}, our new sample has three out of 69 (4 per cent) within the same velocity range. The reason for this is unclear. The low-velocity pulsars should stay close to the Galactic plane and, therefore, be abundant in any radio survey. One possible explanation is that pulsars in the sample by Verbunt et al. (2017) and in the sample by Deller et al. (2019) have different spin-down ages. In Fig. 4, we plot the spin-down ages distribution for these two samples. Overall, the Deller et al. (2019) sample contains fewer objects with $\tau < 10$ Myr and more older objects.

To check if an addition of secondary Maxwellian is significant, we compute the likelihood difference $d\mathcal{L} = 10$ that is equivalent to $\Delta\chi^2 = 99.3$ per cent for two degrees of freedom corresponding to two added parameters. This likelihood difference is very significant, but the significance decreased slightly in comparison to one found by Verbunt et al. (2017). We suspect that this decrease is caused by dearth of low-velocity pulsars in Deller et al. (2019) sample in comparison to the previous measurements.

Further, we introduce a mixed model: 17 pulsars with nominal $|z| < 50$ pc and pulsars with the spin-down age $\tau > 50$ Myr are analysed using an isotropic distribution and all other are analysed

Table 2. Results of maximum likelihood analysis for 69 pulsars in our master list (A) and for the 21 youngest pulsars ($\tau < 3$ Myr; Y). Parameters h and H are used for the Galactic distribution of pulsars $f_D(D)$. Range is the 68 per cent confidence interval.

h	H		Sample		Single Maxwellian			Two Maxwellians						
				N	σ	Range	$d\mathcal{L}$	σ_1	Range	σ_2	Range	w	Range	$d\mathcal{L}$
0.33	1.7	Isotropic models	A	69	229	215–245	≡0	146	125–162	317	277–346	0.58	0.47–0.68	10
0.32	0.8	Isotropic models	A	69	229	215–245	34	152	129–165	324	282–356	0.62	0.51–0.71	42
0.33	1.7	Mixed models	A	17+52	225	210–246	34	128	110–150	298	270–326	0.42	0.27–0.59	43
0.33	1.7	Isotropic models	Y	21	298	266–336	≡0	55	40–80	334	293–384	0.19	0.10–0.30	6
0.18	0.7	Isotropic models	Y	21	290	259–326	28	55	40–80	325	286–374	0.19	0.10–0.30	34
0.33	1.7	Mixed models	Y	6+15	298	266–334	18	70	50–113	328	288–375	0.17	0.08–0.29	21
0.33	1.7	J0614+2229 (isotropic) other mixed	Y	7+14	295	264–332	19	56	41–81	336	291–381	0.20	0.10–0.31	25

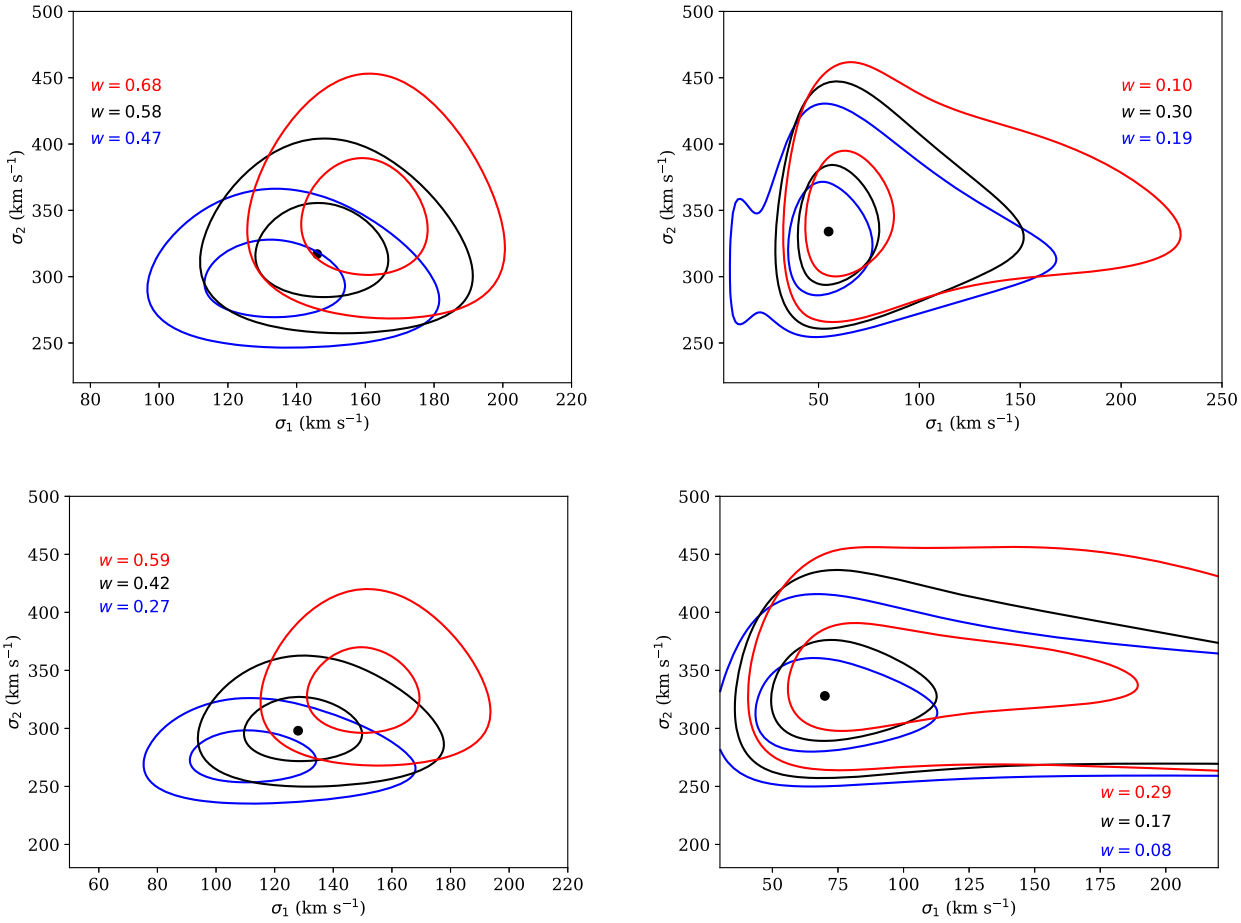

Figure 5. Contour of $d\mathcal{L}(\sigma)$ for fixed values of w for all pulsars in our sample (left-hand column) and only young radio pulsars ($\tau < 3$ Myr; right-hand column). In the upper row we show results for isotropic model and in lower row we show results for the mixed model.

using a semi-isotropic distribution. The calculations of the semi-isotropic model used in Verbunt et al. (2017) have to be slightly corrected to deal with much smaller errors for proper motions in the sample by Deller et al. (2019). Namely, the parameter h responsible for size of the region for the numerical integration (see appendix C in Verbunt et al. 2017) is decreased to $h = 2\pi/500$.

For single mixed Maxwellian we obtain $\sigma = 225^{+21}_{-15}$, for the mixed bimodal Maxwellian distribution we get following parameters: $w = 42^{+17}_{-15}$, $\sigma_1 = 128^{+22}_{-18}$ km s^{-1} and $\sigma_2 = 298 \pm 28$ km s^{-1}. We notice that when the mixed model is used, we obtain significantly lower values of the likelihood ($d\mathcal{L} = 34$ for single Maxwellian and $d\mathcal{L} = 43$ for bimodal Maxwellian). It means that younger pulsars outside of the $|z| < 50$ pc region indeed have preferable orientation of the velocity vector pointing outside of the Galactic plane as it is expected. Application of the mixed model shifts w, σ_1, and σ_2 to slightly lower values. In the case of bimodal Maxwellian, the mixed model keeps correlations between w and σ_1, see Fig. 5 (lower left-hand panel). The mixed bimodal Maxwellian model suggested in Verbunt et al. (2017) is outside of the 99 per cent confidence interval. Addition of the second Maxwellian is significant because the likelihood difference of $d\mathcal{L} = 9$ is equivalent to $\Delta\chi^2 \approx 98.9$ per cent for two degrees of freedom. Therefore, introduction of the mixed model does not change the result qualitatively, but slightly shifts velocities to smaller values.

4.2 Natal kicks of radio pulsars

Studying the natal kick distribution requires us to restrict the sample to the youngest radio pulsars, which are less affected by observational selection and deceleration in the Galactic gravitational potential. On the one hand, it is better to choose as small cut-off for spin-down ages as possible. The fastest pulsars ($\approx$1000 km s^{-1}) could travel up to 1 kpc per 1 Myr. Therefore, such pulsars could escape most modern radio surveys that concentrate on objects close to the Galactic plane. On the other hand, choosing inappropriately small age cut-off we unnecessary decrease the sample size. With this in mind, we decrease the cut-off age to 3 Myr (cut-off used by Hobbs et al. 2005) in comparison to 10 Myr used in Verbunt et al. (2017). Our Y sample contains 21 objects that is comparable in size to Y sample from Verbunt et al. (2017).

We perform multiple tests using the population synthesis code and additional filtration of radio pulsars to check if the velocity estimate works reliably when the observational selection is present. These tests are summarized in Appendix B. We find that the method estimates the parameters of the natal kick velocity distribution reliably even if the selection is present. Moreover, $d\mathcal{L} \geq 6$ means a confident detection of the bimodality. From our tests it become clear that $d\mathcal{L} > 2$ is already significant at >90 per cent level. The maximum likelihood estimates found for synthetic catalogues are not biased and well within expected confidence intervals.

When we optimize the likelihood function using the single isotropic Maxwellian velocity distribution with sample of young pulsars we find that $\sigma = 298^{+38}_{-32}$ km s^{-1}. The values found by Hobbs et al. (2005) and Verbunt et al. (2017) (single Maxwellian $\sigma = 277$ km s^{-1}) are within our 68 per cent confidence interval. It is worth noting that this value is significantly higher than $\sigma = 229^{+16}_{-14}$ km s^{-1} found for the entire sample. This effect is likely a combination of the observational selection mentioned above and physical deceleration of pulsars in the Galactic gravitational potential.

When we optimize the model containing bimodal Maxwellian distribution, we find a result within the 68 per cent confidence interval of Verbunt et al. (2017). The first Maxwellian with $\sigma_1 = 55^{+25}_{-15}$ km s^{-1} contains 19^{+11}_{-9} per cent of all objects and the second Maxwellian with $\sigma_2 = 334^{+50}_{-41}$ km s^{-1} contains 81^{+9}_{-11} per cent of all pulsars. The presence of a second component is quite significant: the likelihood difference $d\mathcal{L} = 6$ corresponds to $\Delta\chi^2 = 95$ per cent for two degrees of freedom.

It is also worth noting that correlation between σ_1 and w is practically negligible, see Fig. 5 (upper right-hand panel). All three contours cover practically the same area, which includes the maximum likelihood point. It indicates that the low- and high-velocity pulsars probably belong to clearly distinguished distributions.

When we optimize the mixed model with single Maxwellian we obtain $\sigma = 298^{+36}_{-32}$ with $d\mathcal{L} = 18$ in comparison to single isotropic Maxwellian case. This model does not have any additional parameters. It means that the younger pulsars are clearly moving away from the Galactic plane.

The bimodal mixed Maxwellian has following parameters: $w = 17^{+12}_{-9}$, $\sigma_1 = 70^{+43}_{-20}$ km s^{-1}, and $\sigma_2 = 328^{+47}_{-40}$ km s^{-1}. The parameters of bimodal mixed Maxwellian model are well within the 68 per cent confidence interval of the isotropic model. The contours of constant likelihood are in Fig. 5 (lower right-hand panel) resemble one found for the isotropic model with an exception of their much longer tails in the high-velocity direction.

We were puzzled by the likelihood difference of this model $d\mathcal{L} = 21$ that is just $d\mathcal{L} = 3$ different from the single Maxwellian mixed model. Such a difference indicates only a slight preference ($\Delta\chi^2 = 77.7$ per cent for two degrees of freedom).[3] However, it is worth remembering that this model is based on at least two essential assumptions: (1) the velocity distribution is a sum of two Maxwellians and (2) the velocity vectors of young pulsars (beside ones in the 50 pc stripe along the Galactic plane) are directed away from the plane. It seems that the second assumption plays an essential role in decreasing the likelihood difference. We plot the likelihood contributions of individual pulsars in Fig. 6 and immediately notice that the mixed model containing two Maxwellians is in all cases better or comparable to two isotropic Maxwellians model except the case of PSR J0614+2229.

PSR J0614+2229 has $\tau = 8.93 \times 10^4$ yr and $B = 4.5 \times 10^{12}$ G estimated by magnetodipole equation and nominal $z = \sin b/\varpi' = 148$ pc. Therefore, the PSR J0614+2229 should move away from the Galactic plane, while in reality it has a significant component of proper motion directed toward the plane. This is a reason why the significance of the mixed model with two Maxwellians is not high enough. Another object in the Y list that seems to move toward the plane is PSR J0538+2817. Both models have exactly the same likelihood for this pulsar that means that its proper motion

[3]If we use assumption that the likelihood ratio test follows χ^2 distribution precisely, but this result seems more significant if we take into account the results of Monte Carlo tests.

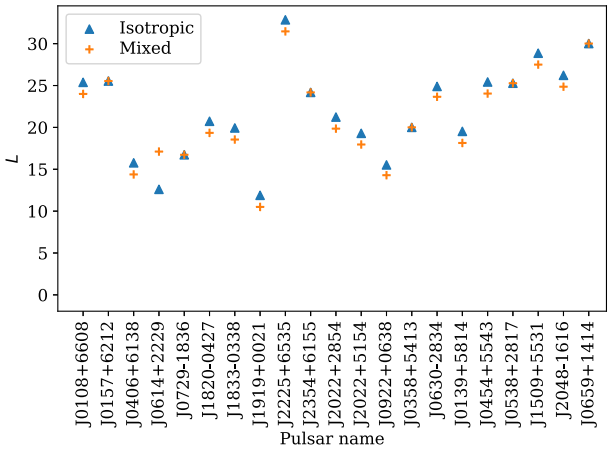

Figure 6. Comparison of individual contribution to the maximum likelihood for sample of radio pulsars with $\tau < 3$ Myr. PSR J0614+2229 seems to strongly prefer isotropic model. To compute both likelihoods we use parameters $w = 0.19$, $\sigma_1 = 55$, and $\sigma_2 = 334$.

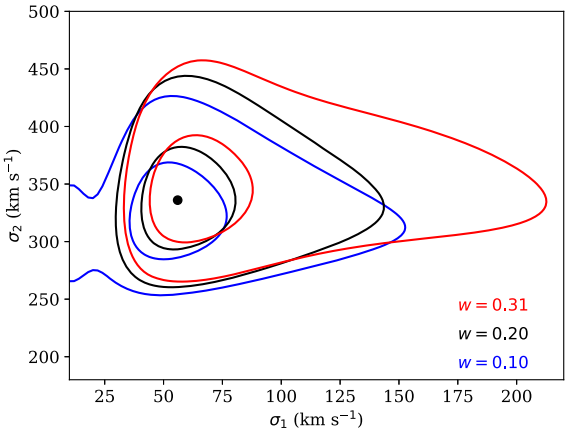

Figure 7. Contours of $d\mathcal{L}(\sigma)$ for Y sample and mixed model where PSR J0614+2229 is treated as one drawn from the isotropic velocity distribution.

toward the plane is apparent. This is not the case, however, for PSR J0614+2229.

We perform additional analysis moving PSR J0614+2229 into the isotropic list and obtain $w = 20^{+11}_{-10}$, $\sigma_1 = 56^{+25}_{-15}$ km s^{-1}, and $\sigma_2 = 336 \pm 45$ km s^{-1}. The results of likelihood optimization in this case are well within 68 per cent confidence interval of the original mixed model. We plot the likelihood profile in Fig. 7. The plot is very similar to the isotropic case: long tails in the high-velocity direction seen in the original mixed model disappeared. This model's total likelihood is significantly different. A mixed model with two Maxwellians with PSR J0614+2229 treated as a pulsar with velocity drawn from the isotropic velocity distribution is significantly more accurate than similar model that contains single Maxwellian ($d\mathcal{L} = 6$ corresponds to $\Delta\chi^2 = 95$ per cent for two degrees of freedom). Therefore, we conclude that PSR J0614+2229 has to be treated as an exception.

It is worth noting that the main reason our original mixed model with two Maxwellians is not as significant as new model is because the orientation of the velocity vector of PSR J0614+2229 is unexpected. If we completely remove PSR J0614+2229 from the sample, we obtain same significance as in the case when we treat

Table 3. Results of the maximum likelihood optimization for parameters determining the Galactic distribution of radio pulsars for different samples. Sample A includes all radio pulsars, sample I includes only ones with $\tau <$ 10 Myr, and sample Y includes only with $\tau < 3$ Myr. Range is 68 per cent confidence interval.

Sample	h (kpc)	Range	H (kpc)	Range
A	0.32	0.3–0.37	0.8	0.72–0.9
I	0.22	0.19–0.25	0.85	0.74–0.97
Y	0.18	0.15–0.23	0.70	0.59–0.87

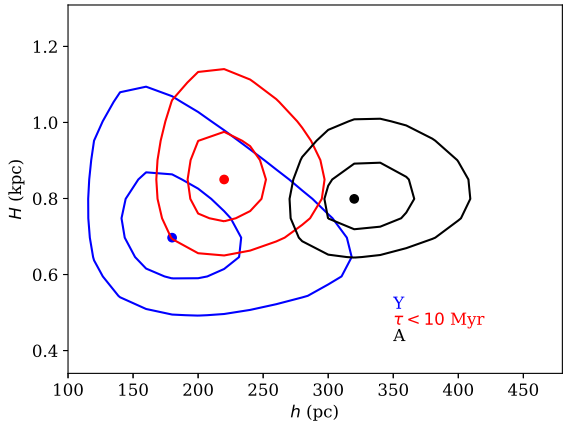

Figure 8. Contours of $d\mathcal{L}(\sigma)$ in the plane of h and H for A, I, and Y samples.

this pulsar as one with velocity drawn from the isotropic velocity distribution.

We run two additional optimizations for the case when $\varpi'/\sigma_\varpi > 2$ and $\tau < 3$ Myr, which adds one additional pulsar to the list. In the case of a single isotropic Maxwellian we get $\sigma = 295^{+37}_{-31}$ km s^{-1}. In the case of the sum of two isotropic Maxwellians we get $w = 0.17^{+11}_{-9}$, $\sigma_1 = 54^{+26}_{-15}$ km s^{-1} and $\sigma_2 = 327^{+47}_{-39}$ km s^{-1}. The bimodal isotropic Maxwellians is more significant than a single Maxwellian with $d\mathcal{L} = 5$, which corresponds to 92 per cent probability. In comparison to our original result the shift in velocity estimates is about a few km s^{-1} and well within our confidence interval estimates.

4.3 Galactic distribution of radio pulsars

We study the dependence of our maximum likelihood technique on parameters of the Galactic distribution of radio pulsars. To do so, we optimize the single isotropic Maxwellian model for values of h and H from equation (2) computed on a grid. We perform this optimization for A and Y samples and also for pulsars with $\tau <$ 10 Myr (sample I hereafter). Results are summarized in Table 3 and in Fig. 8.

We use the optimized values to estimate the parameters of the natal kick, see fifth line in Table 2. Despite a dramatic change in value of parameters h and H the result of the maximum likelihood optimization for velocity distribution is well within the 68 per cent confidence interval of original models, and parameters differ by less than 10 km s^{-1} (see Table 2). This is related to the fact that parallaxes are measured with high precision in new PSRπ catalogue, therefore, the initial distance distribution does not have a significant effect on velocities.

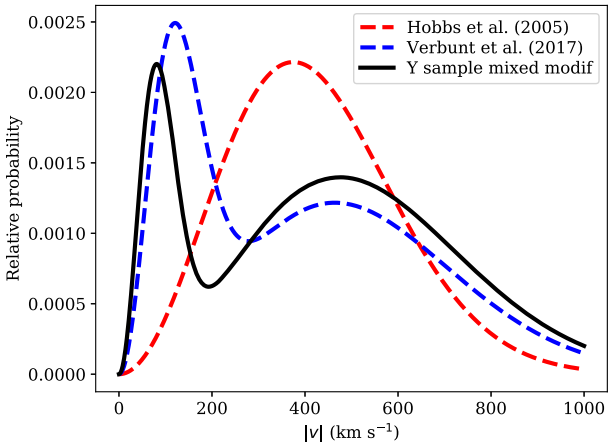

Figure 9. The probability density functions for natal kicks found in different studies. Black solid line shows the distribution found for young radio pulsars using the mixed model with an exception of PSR J0614+2229 that is treated as drawn from the isotropic velocity distribution. Red dashed line shows the distribution found by Hobbs et al. (2005) and blue dashed line shows one found by Verbunt et al. (2017).

Our tests using the pulsar population synthesis code (see Appendix B) show that the values of h and H are very sensitive to exact distribution of latitudes of measured pulsars. In particular, if pulsars are too concentrated toward the Galactic plane, the method tends to give smaller h values. On the other hand, even if the values of h and H are biased, the method estimates parameters of the velocity distribution correctly.

5 DISCUSSION

In Fig. 9, we plot the result of our analysis and two works mentioned previously. Our result differs significantly from the Hobbs et al. (2005) and more similar to work by Verbunt et al. (2017). In comparison to this latter research, the first peak of the velocity distribution has shifted slightly toward even smaller velocities, the height of the first peak decreased and the gap between two modes becomes more apparent. Using our best model for velocities of young radio pulsars, we plot the fraction of NSs born with $v <$ 60 km s^{-1} in Fig. 10. This fraction varies between 2 and 8 per cent and is compatible with one found before in Verbunt et al. (2017).

It is important to highlight once again that our analysis is based only on parallaxes and proper motion measured for *isolated* radio pulsars.[4] If a weak natal kick (0–60 km s^{-1}) occurs more frequently (or solely) in interacting binaries, the binary often stays bound and, therefore, is excluded from our master list. There are a number of theoretical mechanisms suggested in support of this scenario, such as the electron capture supernova explosion or accretion-induced WD collapse. The kick amplitude might be related to an amount of mass lost during the explosion, so a stripped star in an interacting binary would receive much weaker kick and ends up as an isolated pulsar only in exceptional cases. With further constraints on natal kick distributions derived for merging double NS systems (see e.g. Mapelli & Giacobbo 2018), MSPs and BeX binaries, it is important to check if the tension between results of our method and those measurements keeps growing. If it is the case, the preferable

[4]See, for example, Igoshev & Perets (2019) for search for ultrawide companions for these objects.

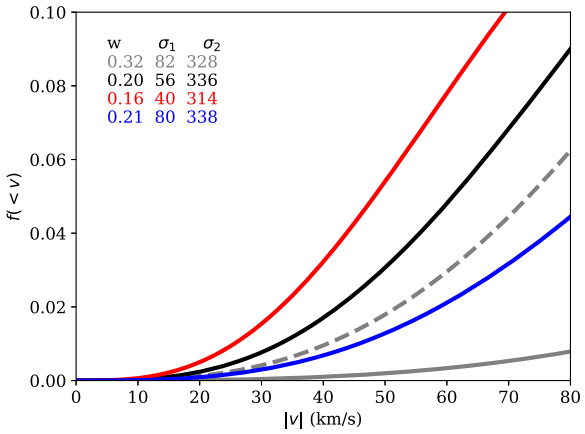

Figure 10. Fraction of young radio pulsars with velocities less than $|v|$. Solid black line shows the best mixed model for Y sample, and red and blue solid lines show the best models for variations of σ_1. The grey dashed line shows results from Verbunt et al. (2017) and dashed solid line is for distribution by Hobbs et al. (2005) with $\sigma = 265$ km s^{-1}.

binary origin of weak natal kicks seems to be the most plausible explanation.

There is an additional caveat in our analysis. The Galactic gravitational potential affects velocity of isolated neutron stars. Stars moving at the highest speeds (>500 km s^{-1}) leave the Galaxy or become a part of the Galactic halo. On the other hand, the only quantity that is available for us to distinguish between older and younger pulsars is the spin-down age. This age is affected by the magnetic field evolution and initial periods. If we assume that our understanding of these two quantities is reasonable, we do not expect the spin-down age to be extremely different from the actual age (e.g. there cannot be a young pulsar with $\tau = 1$ Gyr). However, if there is an unknown mechanism that mixes spin-down ages, e.g. the magnetic field re-emergence after a fall-back (Igoshev, Elfritz & Popov 2016), our selection of youngest pulsars can be more strongly affected by the observational selection.

It is worth to discuss the case of PSR J0614+2229. There are two possible explanations for its abnormal velocity vector directed toward the Galactic plane: (1) pulsar was born high above the plane or (2) pulsar experienced unusual magnetic field evolution. In the first case the pulsar might have been a part of a massive binary system that received large systemic velocity (order of 100 km s^{-1}) during the first supernova explosion. In this case the binary had some time to travel away from the Galactic plane before the secondary supernova explosion. The secondary explosion producing the observed pulsar disrupted the binary. In the second case, PSR J0614+2229 might be a pulsar with a hidden magnetic field that has remerged over time that makes the simple spin-down age estimate extremely unreliable.

6 CONCLUSION

We analysed new parallaxes and proper motion measurements for isolated radio pulsars published by Deller et al. (2019) together with older measurements using the maximum likelihood method. We optimized the parameters of velocity distribution of pulsars. Our findings are as follows.

The velocity distribution of pulsars of all ages presented in our master list is compatible with a bimodal Maxwellian with contribution of first mode $w = 0.42^{+0.17}_{-0.15}$, $\sigma_1 = 128^{+22}_{-18}$ km s^{-1}, and second mode $\sigma_2 = 298 \pm 28$ km s^{-1}. It differs from results of Verbunt et al. (2017) and might be explained by a different selection of pulsars in Deller et al. (2019) in comparison to earlier works. The presence of bimodality is significant at the level of 99.3 per cent.

The natal kick distribution of NSs derived as the velocity distribution of young radio pulsars ($\tau < 3$ Myr) can be described as bimodal Maxwellian with $w = 0.2^{+0.11}_{-0.10}$, $\sigma_1 = 56^{+25}_{-15}$ km s^{-1}, and $\sigma_2 = 336 \pm 45$ km s^{-1}. This distribution lies well within the 68 per cent confidence interval of the distribution found by Verbunt et al. (2017). The presence of bimodality is significant at the level of 95 per cent.

We perform multiple Monte Carlo simulations using a code for the pulsar population synthesis and show that the observational selection does not affect the estimated parameters of the natal kick distribution.

The results of the maximum likelihood method for parameters of velocity distribution are weakly sensitive to the exact value of h and H used and changes are within 10 km s^{-1} if alternative values are assumed.

The fraction of radio pulsars born with $|v| < 60$ km s^{-1} are 5 ± 3 per cent in our best model.

We notice that PSR J0614+2229 with spin-down age $\tau \approx 9 \times 10^4$ yr moves toward the Galactic plane from its nominal height of $z \approx 150$ pc. It could indicate a complicated binary origin of this radio pulsar or its non-standard magnetic field evolution.

ACKNOWLEDGEMENTS

API acknowledges the guidance and help he received from Professor Eric Cator and Professor Frank Verbunt while working on codes used in this research. API thanks the Science and Technology Facilities Council grant ST/S000275/1. API is grateful to Professor S. B. Popov and A. Frantsuzova for fruitful discussions about this paper. API thanks anonymous referee for multiple comments that helped to improve the paper significantly.

REFERENCES

Abbott B. P. et al., 2017, ApJ, 850, L40
Arzoumanian Z., Chernoff D. F., Cordes J. M., 2002, ApJ, 568, 289
Brisken W. F., Benson J. M., Goss W. M., Thorsett S. E., 2002, ApJ, 571, 906
Brisken W. F., Fruchter A. S., Goss W. M., Herrnstein R. M., Thorsett S. E., 2003, AJ, 126, 3090
Chatterjee S., Cordes J. M., Lazio T. J. W., Goss W. M., Fomalont E. B., Benson J. M., 2001, ApJ, 550, 287
Chatterjee S., Cordes J. M., Vlemmings W. H. T., Arzoumanian Z., Goss W. M., Lazio T. J. W., 2004, ApJ, 604, 339
Chatterjee S. et al., 2009, ApJ, 698, 250
Cordes J. M., Lazio T. J. W., 2002, preprint (astro-ph/0207156)
Cordes J. M., Romani R. W., Lundgren S. C., 1993, Nature, 362, 133
Deller A. T., Tingay S. J., Bailes M., Reynolds J. E., 2009, ApJ, 701, 1243
Deller A. T. et al., 2019, ApJ, 875, 100
Edwards R. T., Bailes M., van Straten W., Britton M. C., 2001, MNRAS, 326, 358
Faucher-Giguère C.-A., Kaspi V. M., 2006, ApJ, 643, 332
Frail D. A., Goss W. M., Whiteoak J. B. Z., 1994, ApJ, 437, 781
Hobbs G., Lorimer D. R., Lyne A. G., Kramer M., 2005, MNRAS, 360, 974
Holland-Ashford T., Lopez L. A., Auchettl K., Temim T., Ramirez-Ruiz E., 2017, ApJ, 844, 84
Hu M., Lachin J. M., 2003, Commun. Stat.: Simulation Comput., 32, 619
Hurley J. R., Pols O. R., Tout C. A., 2000, MNRAS, 315, 543
Igoshev A. P., 2017, PhD thesis, Radboud University, Nijmegen, the Netherlands

Igoshev A. P., 2019, MNRAS, 482, 3415
Igoshev A. P., Kholtygin A. F., 2011, Astron. Nachr., 332, 1012
Igoshev A.P., Elfritz J.G., Popov S.B., 2016, MNRAS, 462, 3689
Igoshev A. P., Perets H. B., 2019, MNRAS, 486, 4098
Igoshev A. P., Popov S. B., 2013a, MNRAS, 432, 967
Igoshev A. P., Popov S. B., 2013b, MNRAS, 434, 2229
Igoshev A., Verbunt F., Cator E., 2016, A&A, 591, A123
Kirsten F., Vlemmings W., Campbell R. M., Kramer M., Chatterjee S., 2015, A&A, 577, A111
Kuijken K., Gilmore G., 1989, MNRAS, 239, 651
Kuranov A. G., Popov S. B., Postnov K. A., 2009, MNRAS, 395, 2087
Lorimer D. R. et al., 2006, MNRAS, 372, 777
Lyne A. G., Lorimer D. R., 1994, Nature, 369, 127
Manchester R. N. et al., 2001, MNRAS, 328, 17
Manchester R. N., Hobbs G. B., Teoh A., Hobbs M., 2005, AJ, 129, 1993
Mapelli M., Giacobbo N., 2018, MNRAS, 479, 4391
Ostriker J. P., Rees M. J., Silk J., 1970, Astrophys. Lett., 6, 179
Pfahl E., Rappaport S., Podsiadlowski P., Spruit H., 2002, ApJ, 574, 364
Podsiadlowski P., Pfahl E., Rappaport S., 2005, in Rasio F. A., Stairs I. H., eds, ASP Conf. Ser. Vol. 328, Binary Radio Pulsars. Astron. Soc. Pac., San Francisco, p. 327
Popov S. B., Colpi M., Treves A., Turolla R., Lipunov V. M., Prokhorov M. E., 2000, ApJ, 530, 896
Popov S. B., Postnov K. A., Shakura N. I., 2015, MNRAS, 447, 2817
Predehl P. et al., 2011, Proc. SPIE, 8145, 81450D
Shvartsman V. G., 1971, SvA, 14, 662
Tauris T. M. et al., 2017, ApJ, 846, 170
Toonen S., Perets H. B., Igoshev A. P., Michaely E., Zenati Y., 2018, A&A, 619, A53
Townsend L. J., Coe M. J., Corbet R. H. D., Hill A. B., 2011, MNRAS, 416, 1556
Verbiest J. P. W., Weisberg J. M., Chael A. A., Lee K. J., Lorimer D. R., 2012, ApJ, 755, 39
Verbunt F., Cator E., 2017, J. Astrophys. Astron., 38, 40
Verbunt F., Igoshev A., Cator E., 2017, A&A, 608, A57
Yao J. M., Manchester R. N., Wang N., 2017, ApJ, 835, 29

APPENDIX A: LIST OF PULSARS

Table A1. Ref. is the number from the Table 1. An 'i' in the third column indicates that an isotropic velocity distribution was used to model this particular pulsar in the mixed velocity model. For PSR J0614+2229 the isotropic model was used only in one case, see Section 4.2 for details.

B-name	J-name		l (°)	b (°)	P (s)	$\log\tau$ (yr)	$\mu_{\alpha*,o}\,\sigma_\alpha$ (mas yr^{-1})	$\mu_{\delta,o}\,\sigma_\delta$ (mas yr^{-1})	$\varpi\,\sigma_\varpi$ (mas)	Ref.
B0031–07	J0034–0721		110.42	− 69.82	0.94295	7.56	10.37(8)	− 11.13(16)	0.93(8)	6
B0052+51	J0055+5117		123.62	− 11.58	2.11517	6.55	10.490(85)	− 17.352(204)	0.349(55)	8
B0059+65	J0102+6537		124.08	2.77	1.67916	6.65	9.252(81)	1.828(206)	0.399(45)	8
B0105+65	J0108+6608		124.65	3.33	1.28366	6.19	− 32.754(36)	35.162(51)	0.468(35)	8
B0136+57	J0139+5814		129.22	− 4.04	0.27245	5.61	− 19.11(7)	− 16.60(7)	0.37(4)	6
B0144+59	J0147+5922		130.06	− 2.72	0.19632	7.08	− 6.380(101)	3.826(97)	0.495(93)	8
B0154+61	J0157+6212	i	130.59	0.33	2.35174	5.3	1.521(105)	44.811(48)	0.554(39)	8
B0320+39	J0323+3944	i	152.18	− 14.34	3.03207	7.88	26.484(59)	− 30.780(29)	1.051(40)	8
B0329+54	J0332+5434	i	145.0	− 1.22	0.71452	6.74	16.969(29)	− 10.379(58)	0.595(25)	8
B0331+45	J0335+4555	i	150.35	− 8.04	0.2692	8.76	− 3.638(73)	− 0.097(134)	0.409(27)	8
B0353+52	J0357+5236	i	149.1	− 0.52	0.19703	6.82	13.908(115)	− 10.633(98)	0.305(77)	8
B0355+54	J0358+5413	i	148.19	0.81	0.15638	5.75	9.20(18)	8.17(39)	0.91(16)	4
B0402+61	J0406+6138		144.02	7.05	0.59458	6.23	12.400(151)	22.716(100)	0.218(57)	8
B0450+55	J0454+5543		152.62	7.55	0.34073	6.36	53.34(6)	− 17.56(14)	0.84(5)	6
	J0538+2817	i	179.72	− 1.69	0.14316	5.79	− 23.57(10)	52.87(10)	0.72(12)	6
B0559–05	J0601–0527		212.2	− 13.48	0.39597	6.68	− 7.348(77)	− 15.227(105)	0.478(45)	8
B0611+22	J0614+2229	i	188.79	2.4	0.33496	4.95	− 0.233(53)	− 1.224(65)	0.282(31)	8
B0626+24	J0629+2415		188.82	6.22	0.47662	6.58	3.629(193)	− 4.607(153)	0.333(54)	8
B0628–28	J0630–2834		236.95	− 16.76	1.24442	6.44	− 46.30(99)	21.26(52)	3.009(409)	5
B0656+14	J0659+1414	i	201.11	8.26	0.38489	5.05	44.07(63)	− 2.40(29)	3.47(36)	2
B0727–18	J0729–1836	i	233.76	− 0.34	0.51016	5.63	− 13.072(125)	13.252(456)	0.489(98)	8
B0809+74	J0814+7429	i	140.0	31.62	1.29224	8.09	24.02(9)	− 43.96(35)	2.31(4)	1
B0818–13	J0820–1350		235.89	12.59	1.23813	6.97	21.64(9)	− 39.44(5)	0.51(4)	6
B0823+26	J0826+2637		196.96	31.74	0.53066	6.69	62.994(21)	− 96.733(85)	2.010(13)	8
B0919+06	J0922+0638		225.42	36.39	0.43063	5.7	18.8(9)	86.40(70)	0.83(13)	3
B0950+08	J0953+0755		228.91	43.7	0.25307	7.24	− 2.09(8)	29.46(7)	3.82(7)	1
B1133+16	J1136+1551		241.9	69.2	1.18791	6.7	− 73.785(31)	366.569(72)	2.687(18)	8
B1237+25	J1239+2453		252.45	86.54	1.38245	7.36	− 106.82(17)	49.92(18)	1.16(8)	1
B1322+83	J1321+8323		121.89	33.67	0.67004	7.27	− 52.674(99)	32.373(204)	0.968(140)	8
B1508+55	J1509+5531		91.33	52.29	0.73968	6.37	− 73.64(5)	− 62.65(9)	0.47(3)	6
B1530+27	J1532+2745		43.48	54.5	1.12484	7.36	1.542(127)	18.932(118)	0.624(96)	8
B1541+09	J1543+0929		17.81	45.78	0.74845	7.44	− 7.61(6)	− 2.87(7)	0.13(2)	6
B1540–06	J1543–0620		0.57	36.61	0.70906	7.11	− 16.774(63)	− 0.312(147)	0.322(45)	8
B1556–44	J1559–4438		334.54	6.37	0.25706	6.6	1.52(14)	13.15(5)	0.384(81)	5
B1604–00	J1607–0032		10.72	35.47	0.42182	7.34	− 26.437(99)	− 27.505(222)	0.934(47)	8

Table A1 – *continued*

B-name	J-name		l (°)	b (°)	P (s)	log τ (yr)	$\mu_{\alpha*,o}\,\sigma_\alpha$ (mas yr^{-1})	$\mu_{\delta,o}\,\sigma_\delta$ (mas yr^{-1})	$\varpi\,\sigma_\varpi$ (mas)	Ref.
B1620–09	J1623–0908		5.3	27.18	1.27644	6.89	– 10.769(131)	23.509(166)	0.586(101)	8
B1642–03	J1645–0317		14.11	26.06	0.38769	6.54	– 1.011(51)	20.523(205)	0.252(28)	8
B1700–18	J1703–1846		3.23	13.56	0.80434	6.87	– 0.751(102)	16.962(230)	0.348(49)	8
B1732–07	J1735–0724		17.27	13.28	0.41933	6.74	0.791(87)	20.614(74)	0.150(41)	8
B1738–08	J1741–0840		16.96	11.3	2.04308	7.15	0.436(126)	6.876(109)	0.279(58)	8
B1753+52	J1754+5201		79.61	29.63	2.3914	7.38	– 3.950(47)	1.101(72)	0.160(29)	8
B1818–04	J1820–0427		25.46	4.73	0.59808	6.18	– 7.318(74)	15.883(88)	0.351(55)	8
B1831–03	J1833–0338		27.66	2.27	0.6867	5.42	– 17.409(158)	15.038(337)	0.408(67)	8
B1839+56	J1840+5640		86.08	23.82	1.65286	7.24	– 31.212(33)	– 29.079(82)	0.657(65)	8
	J1901–0906		25.98	– 6.44	1.78193	7.24	– 7.531(45)	– 18.211(159)	0.510(67)	8
B1911+13	J1913+1400		47.88	1.59	0.52147	7.01	– 5.265(72)	– 8.927(65)	0.185(27)	8
B1917+00	J1919+0021		36.51	– 6.15	1.27226	6.42	10.167(143)	– 4.713(102)	0.166(42)	8
B1929+10	J1932+1059	i	47.38	– 3.88	0.22652	6.49	94.06(9)	43.24(17)	2.78(6)	7
B1935+25	J1937+2544		60.84	2.27	0.20098	6.7	– 10.049(42)	– 13.055(39)	0.318(31)	8
B2003–08	J2006–0807	i	34.1	– 20.3	0.58087	8.3	– 6.176(70)	– 10.616(174)	0.424(101)	8
B2016+28	J2018+2839	i	68.1	– 3.98	0.55795	7.78	– 2.64(21)	– 6.17(38)	1.03(10)	1
B2020+28	J2022+2854		68.86	– 4.67	0.3434	6.46	– 3.46(17)	– 23.73(21)	0.61(8)	7
B2021+51	J2022+5154		87.86	8.38	0.5292	6.44	– 5.03(27)	10.96(17)	0.78(7)	7
B2044+15	J2046+1540	i	61.11	– 16.84	1.13828	8.0	– 10.455(90)	0.681(90)	0.310(82)	8
B2043–04	J2046–0421		42.68	– 27.39	1.54694	7.22	10.760(38)	– 4.404(373)	0.167(42)	8
B2045–16	J2048–1616		30.51	– 33.08	1.96157	6.45	113.16(2)	– 4.60(28)	1.05(3)	6
B2053+36	J2055+3630		79.13	– 5.59	0.22151	6.98	1.04(4)	– 2.46(13)	0.17(3)	6
B2110+27	J2113+2754	i	74.99	– 14.03	1.20285	6.86	– 27.981(52)	– 54.432(96)	0.704(23)	8
B2111+46	J2113+4644		89.0	– 1.27	1.01468	7.35	9.525(148)	8.846(90)	0.454(77)	8
	J2144–3933	i	2.79	– 49.47	8.50983	8.43	– 57.89(88)	– 155.90(54)	6.051(560)	5
B2148+63	J2149+6329		104.25	7.41	0.38014	7.55	15.786(131)	11.255(284)	0.356(72)	8
B2154+40	J2157+4017		90.49	– 11.34	1.52527	6.85	16.13(10)	4.12(12)	0.28(6)	6
B2224+65	J2225+6535		108.64	6.85	0.68254	6.05	147.220(243)	126.532(115)	1.203(204)	8
	J2248–0101		69.26	– 50.62	0.47723	7.06	– 10.548(117)	– 17.407(267)	0.256(67)	8
B2303+30	J2305+3100		97.72	– 26.66	1.57589	6.94	– 3.737(82)	– 15.571(163)	0.223(33)	8
B2310+42	J2313+4253		104.41	– 16.42	0.34943	7.69	24.15(10)	5.95(13)	0.93(7)	6
B2315+21	J2317+2149		95.83	– 36.07	1.44465	7.34	8.522(104)	0.136(192)	0.510(57)	8
	J2346–0609		83.8	– 64.01	1.18146	7.14	37.390(42)	– 20.230(107)	0.275(36)	8
B2351+61	J2354+6155	i	116.24	– 0.19	0.94478	5.96	22.755(56)	4.888(33)	0.412(43)	8

APPENDIX B: TESTING THE METHOD

Some initial tests of the maximum likelihood methods are described in chapter 3 of Igoshev (2017). These tests included limited or absent observational selection. Here we perform new tests taking into account observation selection typical for isolated radio pulsars. For each test we perform following procedure: (1) we generate 10 synthetic catalogues (each containing 21 objects) with fixed velocity distribution and errors similar to ones in our catalogue; (2) we run code for single isotropic Maxwellian model; (3) we run code for bimodal isotropic Maxwellian model; and (4) we compare results of optimization with nominal values. The main question that we try to answer with these tests if the results of the method are indicative of the actual natal kick distribution.

A synthetic catalogue is prepared in following manner: (1) run the population synthesis code for isolated radio pulsars; (2) filter the resulting catalogue selecting close radio pulsars with spin-down ages less than 3 Myr; (3) convert the catalogue in the format accepted by our maximum likelihood code and add random value to parallax and proper motions.

To obtain synthetic pulsars we use the isolated pulsar population synthesis code NINA[5] (Nova Investigii Neutronicorum Astrorum – New Studies of Neutron Stars). Some previous usage and description of this code can be found in Igoshev & Kholtygin (2011) and Igoshev & Popov (2013a,b). The code essentially follows the algorithm described by Faucher-Giguère & Kaspi (2006). There are small changes that we summarize here. The code traces isolated stellar evolution using approximated equations by Hurley, Pols & Tout (2000). Massive stars are born in spiral arms on a circular orbit around the Galactic Centre. Additional velocity is drawn from the Maxwellian velocity distribution with $\sigma = 15$ km s^{-1} to mimic the spread in OB stars velocities. The stellar evolution and motion in the Galactic gravitational potential (Kuijken & Gilmore 1989) is traced up to the supernova explosion. At the moment of supernova explosion a natal kick is imparted to the NS. The velocity vector of the kick is added to the current velocity in the Galactic gravitational potential. The motion of produced NS is integrated further. We populate the Galaxy with NS starting 300 Myr ago. To compute the period and period derivative, we assume that the initial magnetic field

[5]Source code and instructions are available at https://github.com/ignotur/NINA

is drawn from the lognormal distribution with $\mu_B = 12.65$ [$\log_{10}$ G] and $\sigma_B = 0.55$ [$\log_{10}$ G], while the initial periods are drawn from the normal distribution with $\mu_p = 0.25$ s and $\sigma_p = 0.15$ s. We assume that the magnetic field is constant and does not decay. We use all parameters for the radio luminosity as they found by Faucher-Giguère & Kaspi (2006). We perform the same selection as in aforementioned article to identify radio bright pulsars that could have been detected in the Parkes Multibeam Survey or Swinburn Multibeam Survey (Edwards et al. 2001; Manchester et al. 2001).

These synthetic pulsars are located mostly at much larger distances than pulsars with measured parallaxes and proper motions. Therefore, we filter this catalogue selecting a subsample of pulsars, which approximately follows the distance distribution seen in our sample. Namely, we prepare the cumulative distribution of measured parallaxes for stars in our sample. Further for each synthetic pulsar we generate a uniform random value between 0 and 1. If this value is less than the cumulative fraction measured in our sample for the parallax of the synthetic pulsar, we accept the synthetic pulsar in our sample. Otherwise, we disregard it.

At this step we compute galactic coordinates of synthetic pulsars and their proper motions. For consistency, we add a normal distributed variable to actual parallax and proper motion of the pulsar with the standard deviations equal to errors in the real catalogue.

We perform tests for both false positive and false negative rates of our method. The false positive rate is how often the method wrongly claims that the natal kick velocity distribution is bimodal while the actual distribution contains a single Maxwellian. The false negative rate is how often the method claims that the velocity distribution is single Maxwellian while the actual distribution is bimodal.

To study the false positive cases we generate 10 radio pulsar populations with assumed single Maxwellian velocity distribution with $\sigma = 256$ km s^{-1}. For all 10 cases, the single Maxwellian velocity distribution is the preferred velocity distribution. In nine cases we obtain $d\mathcal{L} = 0$ for the sum of two Maxwellians, which means that addition of two parameters does not improve the fit at all. In a single case we obtained $d\mathcal{L} = 1.32$ that does not show any significant improvement in the fit. The estimated values for σ in all cases were within 120 km s^{-1} confidence interval centred at the assumed value. In six out of 10 cases the estimated σ was within 60 km s^{-1} confidence interval. Based on this test we can conclude that the false positive rate of the method is very small ($<$ 10 per cent for $d\mathcal{L} > 1.32$), so the method will not discover bimodal Maxwellian instead of a single Maxwellian. In the real sample we identified two Maxwellians with $d\mathcal{L} = 6$.

To test the false negative rate of the method we performed two tests varying the velocity distribution. In the first test we assumed that the natal kick distribution consists of two Maxwellians with a half of objects drawn from a Maxwellian with $\sigma_1 = 40$ km s^{-1}, while other half is drawn from a Maxwellian with $\sigma_2 = 300$ km s^{-1}. We analyse the synthetic catalogue with our code. The sum of two Maxwellians always gives a closer fit to the distribution. Only in one case we identify $d\mathcal{L} = 3.2$, so it is somewhat small to be absolutely confident in the result. In all other cases $d\mathcal{L} = 12$–28. In the result the estimated fraction of low-velocity objects range from 15 to 62 per cent. Therefore, under these conditions the false negative rate is very small ($<$10 per cent for $d\mathcal{L} > 3.2$).

We test our method for the velocity distribution that was identified as the best model for the natal kick, i.e. we assume that 19 per cent of radio pulsars are drawn from the Maxwellian with $\sigma_1 = 55$ km s^{-1} and remaining 81 per cent is from Maxwellian with $\sigma_2 = 334$ km s^{-1}. In two cases we find that the Maxwellian velocity distribution describes the data from the synthetic catalogue well enough $d\mathcal{L} = 0$. In total of six cases $d\mathcal{L} < 5$, so if we did not know the underlying velocity distribution, we would suggest that this is a simple Maxwellian. Therefore, for the realistic natal kick parameters the false negative rate is quite large ($\approx$60 per cent for $d\mathcal{L} < 5$). Taking into account all results, we can conclude that it is very improbable to find two Maxwellians for the natal kick velocity distribution in the data if only one is present, but it is somewhat probable to find a single Maxwellian in the data even if two Maxwellians are actually present and the contribution of weak natal kicks is small. Overall, severe selection effects imposed on the pulsar population do not seem to affect the result of our analysis for found values of $d\mathcal{L}$.

To test if the method correctly estimates h and H values we proceed in two steps. First of all, we generate a synthetic catalogue following all assumptions of the maximum likelihood technique, so no observational selection. In particular we distributed pulsars isotropically on the sky. In this case the maximum likelihood technique correctly estimated h and H values. Secondly, we use synthetic catalogues from previous test. In these tests, we find that the estimate for h is about of 50–100 pc, while in reality the assumptions of the population synthesis give $h_{\rm true} \approx 300$ pc. The reason for this mismatch is that the pulsars are not distributed uniformly over the Galactic latitude in the population synthesis, but instead follow band with $|b| < 15^\circ$. We try to modify the method using the integrated likelihood approach (Hu & Lachin 2003) for parameters of the velocity distribution and for Galactic latitudes. Both options did not work in our tests. Therefore, we cannot prove that the estimated h and H are indeed correct for our sample.

This paper has been typeset from a TEX/LATEX file prepared by the author.